A Fast Patch-Based Approach for Pseudo-CT Generation from MRI T1-Weighted Images: A Potential Solution for PET/MR Attenuation Correction

Angel Torrado-Carvajal[1,2], Eduardo Alcain[3], Joaquin L. Herraiz[2,4], Antonio S. Montemayor[3], Juan A. Hernandez-Tamames[1,2], Elfar Adalsteinsson[5,6], Larry L. Wald[6,7], and Norberto Malpica[1,2]

[1]Medical Image Analysis and Biometry Lab, Universidad Rey Juan Carlos, Mostoles, Madrid, Spain, [2]Madrid-MIT M+Vision Consortium, Madrid, Spain, [3]Dept. of Computer Science, Universidad Rey Juan Carlos, Mostoles, Madrid, Spain, [4]Research Laboratory of Electronics, Massachusetts Institute of Technology, Cambridge, MA, United States, [5]Dept. of Electrical Engineering and Computer Science, Massachusetts Institute of Technology, Cambridge, MA, United States, [6]Harvard-MIT Health Sciences and Technology, Massachusetts Institute of Technology, Cambridge, MA, United States, [7]Martinos Center for Biomedical Imaging, Dept. of Radiology, MGH, Charlestown, MA, United States

Target Audience: Researchers and clinicians who are interested in hybrid PET/MR attenuation correction techniques.

Purpose: Constructing PET attenuation correction maps (AC maps) for use in hybrid PET/MR systems is challenging because no direct relation exists between PET attenuation coefficients (μ) and MR signal intensity [1]. Constructing a pseudo-CT from only MRI data can help to decrease patient ionization by removing the need of patient-specific CT acquisition. Previous MRI-based approaches include Ultra-short TE (UTE) sequences [2], deformable models [3], and multi-atlas segmentation using label-fusion [4]. Recently, patch-based methods have showed to be a versatile segmentation technique [5]. In this work, we propose a fast pseudo-CT generation from a patient-specific MRI T1-weighted image using a group-wise patch-based approach and a limited MRI and CT atlas dictionary.

Methods: ***Data Acquisition:*** A data set containing 19 MRI-CT pairs from healthy volunteers was used. MRI images of the head were acquired on a General Electric Signa HDxt 3.0T MR scanner using the body coil for excitation and an 8-channel quadrature brain coil for reception. Subjects were positioned supine. Imaging was performed using an isotropic 3DT1w SPGR sequence with a TR=10.024ms, TE=4.56ms, TI=600ms, NEX=1, acquisition matrix=288x288, resolution=1x1x1mm, flip angle=12. CT images were acquired on a Siemens Somatom Sensation 16 CT scanner with matrix=512x512, resolution=0.48x0.48mm, slice thickness=0.75mm, PITCH=0.7mm, acquisition angle=0º, voltage=120kV, radiation intensity=200mA.

Data Preprocessing: Image preprocessing was carried out using 3D Slicer built-in modules [6]. This preprocessing included MRI bias correction (N4 ITK MRI bias correction), rigid registration (general registration BRAINS) to align all the images, and normalization of the grayscale values (ITK-based histogram matching).

Modality Propagation: Patch-based segmentation was developed as an adaptation of the non-local frameworks developments in non-local denoising [7]. Let I_{MR} be an input image to be processed, and $\mathcal{A}$ an anatomy atlas containing a set of MRI T1-weighted volumes $\mathcal{I}_{MR}$ and their corresponding CT volumes $\mathcal{I}_{CT}$: $\mathcal{A}=\{(I^i_{MR},I^i_{CT}), i=1,\ldots,n\}$. Let us consider w_i as a weight reflecting non-local similarities between voxels $\mathbf{x}$ in the input image I_{MR} and voxels $\mathbf{y}$ in the image I^i_{MR} of the atlas $\mathcal{A}$ over the image domain Ω, and computed as described in [5]. In our context, the variations of the anatomical structures in a population are bounded, so we can find good matches in a specific neighborhood $\mathcal{N}(\mathbf{x})$ of a specific voxel $\mathbf{x}$. The weights are then estimated in this local area. Thus, we can obtain an estimation of I_{CT} by taking all the images I^i_{MR} in the atlas $\mathcal{A}$ to produce a group-wise combination of their corresponding I^i_{CT} images. Contrary to registration-based approaches, if there is no correspondence between the patch of the input image I_{MR} and the patches of the images I^i_{MR} in the atlas $\mathcal{A}$, no value (NaN) is asigned to the voxel $\mathbf{x}$ of I_{CT}. This situation makes it necessary to include a regularization step, dealing with non-labeled voxels. Usually these cases are isolated, so in this work we have assigned to this voxel the value of the median in his neighborhood. The size for this neighborhood $\mathcal{N}_2(\mathbf{x})$ has been set to 3 in this paper.

GPU Implementation: The calculation of the label $\mathcal{L}(\mathbf{x})$ for each voxel $I_{MR}(\mathbf{x})$ in the 3D input volume is completely independent from the other voxels, so we have implemented the segmentation algorithm in a Graphics Processing Unit (GPU). Configuring a 3D grid in a CUDA model let us eliminate loops to iterate over the different voxels in the volume. Our CUDA kernel contains the selection of atlas $\mathcal{A}$, and the search in the neighborhood $\mathcal{N}(\mathbf{x})$; in this way, each label calculation is performed in a separate thread.

PET Simulation: We obtained detailed tissue models from the T1-weighted volumes by using the pipeline described in [REF]. These models contained cerebellum WM and GM, brain WM and GM, CSF, skull, eyes, muscle, fat, and skin. We used these models to assign PET activity to each tissue obtaining a ground truth map. Then, these ground truth maps where attenuated using the patient-specific CT (gold standard), and corrected using the estimated pseudo-CT.

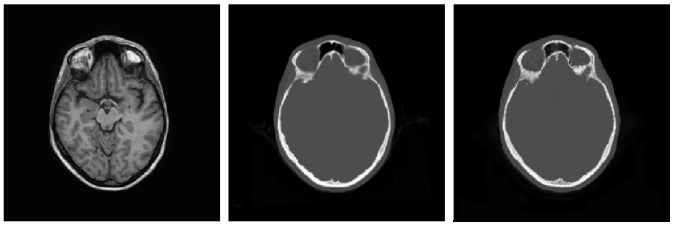

Fig. 1. Axial images of the patient-specific MR (left), patient-specific CT (center), and estimated pseudo-CT using our approach (right).

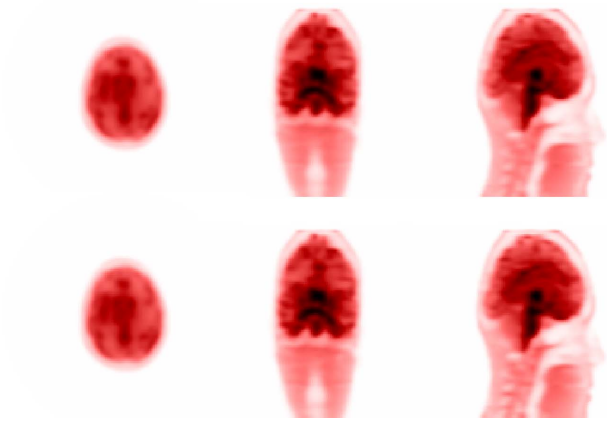

Fig. 2. Simulated ground truth PET activity (first row), and attenuated with the patient-specific CT (gold standard) and corrected with our estimated pseudo-CT PET activity (second row).

Results: The data set was separated into an atlas $\mathcal{A}$ containing 10 MRI-CT pairs $\mathcal{A}=\{(I^i_{MR},I^i_{CT}), i=1,\ldots,10\}$, and a test set $\mathcal{T}$ containing the 9 remaining MRI-CT pairs $\mathcal{T}=\{(I^i_{MR},I^i_{CT}), i=1,\ldots,9\}$. Figure 1 shows the MR, CT and estimated pseudo-CT for one of the subjects participating in this study. Visual inspection evaluation was performed by an expert radiologist to confirm our method accuracy; our pipeline works equally well in all cases considered. The GPU implementation led to a substantial decrease in the computational time making the approach suitable for real applications. Figure 2 shows the simulated ground truth PET activity, and the attenuated and corrected activity.

Discussion: The use of patch-based techniques to estimate a pseudo-CT from MR T1-weighted images allows determining accurate AC maps for use in hybrid PET/MR systems. The proposed method provides an accurate estimation of the pseudo-CT with a similar accuracy as patient-specific CT does. This avoids the over-simplification of most previous proposed methods based on segmented MR images that assume that all voxels in the same tissue type should have the same attenuation coefficients. The use of this post-processing approach may decrease the scanning time compared to UTE approaches, improving the use of MRI scanners.

Conclusion: MRI-based AC maps estimation for use in hybrid PET/MR systems is a challenging task. Due to the nature of MR no direct relation exists between PET attenuation coefficients and MR signal intensity. In this work we have described an approach for the estimation of a pseudo-CT by using a fast patch-based approach based on a single T1-weighted MRI image of a subject as input. The estimation of the pseudo-CT based only on the patient-specific MRI is feasible with this approach. The results are promising and may describe a potential solution for PET/MR attenuation correction. This approach can also be used in other applications such as SAR management and hotspot suppression in parallel transmit MRI.

References: [1] Wagenknecht, W. et al. Magn Reson Mater Phy 2013, 26(1):99–113. [2] Keereman, V. et al. J Nucl Med 2010, 51(5):812–818. [3] Wang, D. et al. JMRI-J Magn Reson Im 2009, 30(3):490–498. [4] Torrado-Carvajal, A. et al. Proc. ISMRM 2014, 22:1177. [5] Rousseau, F. et al. IEEE T Med Imaging 2011, 30(10):1852–1862. [6] Pieper, S. et al. Proc. ISBI 2004, 1:632–635. [7] Katkovnik, V. et al. Int J Comput Vision 2010, 86(1):1–32. [8] Torrado-Carvajal, A. et al. Proc. ISMRM 2014, 22:4906.

Acknowledgements: This project is supported by the Comunidad de Madrid and the Madrid MIT M+Vision Consortium.